Polymer 51 (2010) 4152–4159

Contents lists available at ScienceDirect

Polymer

journal homepage: www.elsevier.com/locate/polymer

Toughness and fracture energy of PDMS bimodal and trimodal networks with widely separated precursor molar masses

Geoffrey D. Genesky, Claude Cohen*

School of Chemical and Biomolecular Engineering, Olin Hall, Cornell University, Ithaca, NY 14850, USA

ARTICLE INFO

Article history:
Received 13 May 2010
Received in revised form
28 June 2010
Accepted 30 June 2010
Available online 7 July 2010

Keywords:
Bimodal networks
Trimodal networks
Enhanced toughness

ABSTRACT

End-linked PDMS bimodal and trimodal networks display enhanced mechanical properties in uniaxial extension over those of unimodal networks with similar modulus when the molar masses of their precursor chains are widely separated. These multimodal networks have optimal mechanical properties when the short chains are near their overlap concentration and sustain most of the load, but the volume of the system is still dominated by the ductile long chain component. Such elastomers can be stretched to large elongations before fracture while displaying an upturn in stress at high strain. Improvement in fracture energy of pre-cut bimodal and trimodal networks over that of unimodal networks is much less pronounced and appears to be dictated by the average molar mass of the effective elastic strands in each network.

1. Introduction

Bimodal polymer networks are produced by combining and end-linking two sets of telechelic chains of different molar masses. These end-linked elastomers have attracted a great deal of interest since they often show enhanced mechanical properties when the two precursor molar masses are widely separated [1]. For instance, bimodal networks often absorb a greater energy before failure (toughness) than unimodal networks, and can display a distinct upturn in stress when deformed to high elongation ratios [2]. This stress upturn has often been attributed to an increased loading on the short chains, whose stress increases as they approach their limited extensibilities [2–7]. These authors speculate that the presence of the long chains also allows optimal bimodal networks to be stretched to large elongations before fracture. This proposed mechanism for reinforcement suggests that elastomers with three distinct precursor molar mass distributions could provide a further advancement in mechanical properties. Such trimodal networks would have chemically-identical short, medium, and long chains cross-linked into the same structure. Addition of the medium precursor molar mass would add a more flexible component than the brittle short chains, while still contributing to the stress upturn as the network was stretched to increased elongation ratios.

Despite the potential of trimodal networks, very few studies of these types of materials have been published. The first experimental investigations of trimodal polydimethylsiloxane (PDMS) networks revealed a disappointing stress–strain performance. The elastomers studied were quite brittle since the long chain molar mass was only 18,000 g/mol [8]. Subsequent theoretical calculations indicated that trimodal networks can outperform unimodal or bimodal elastomers because they can store an increased amount of elastic free energy before the network chains are stretched to their maximum extensibilities [9]. These calculations revealed that trimodal networks would be particularly attractive if the long chain was quite long (with molar mass ~100,000 g/mol) and the three precursor molar masses were widely separated (each by at least a factor of 10). More recently, multiple quantum NMR (MQ-NMR) experiments have demonstrated that filled trimodal PDMS networks can show two or three distributions of residual dipolar couplings when in the unstrained state [10,11], indicating multiple domains of residual chain segment order. These results appear to be consistent with MQ-NMR studies of bimodal networks that found a distinct residual dipolar coupling from both the short chains and the long chains [12,13]. Having recently related ^{2}H NMR multiple chain segment orientations in bimodal networks to their improved mechanical properties [6], we expect trimodal networks with two or three distributions of segment order should be capable of absorbing a high energy before fracture.

In this paper, we investigate PDMS multimodal network properties through two types of experiments: uniaxial extension (simple extension) testing, and cut growth tests on samples with

* Corresponding author. Tel.: +1(607) 255 7292; fax: +1(607) 255 9166.
E-mail address: cc112@cornell.edu (C. Cohen).

0032-3861/$ – see front matter © 2010 Elsevier Ltd. All rights reserved.
doi:10.1016/j.polymer.2010.06.054

pure shear (constrained shear) geometries. Mechanical properties for unimodal, bimodal, and trimodal networks with similar molar mass between effective cross-links M_c are compared to assess the degree of improvement brought about by increasing the number of molar mass distributions in the elastomers. Cut growth test fracture energies of unimodal networks are analyzed using the classical Lake-Thomas theory [14]. Improvement in toughness [defined in section 2.2] values of multimodal over unimodal networks measured via simple extension experiments is contrasted to improvement in fracture energy from cut growth tests. A previously proposed mechanism for mechanical reinforcement in bimodal networks [15] is extended to trimodal networks and is utilized to explain the results of each type of experiment.

2. Experimental

2.1. Materials

All vinyl-terminated PDMS chains were synthesized via methods detailed in an earlier publication [15] except for the 800 g/mol chains, which were purchased from Gelest, Inc. Molar masses M_n and polydispersity indices of the precursor chains were determined by gel permeation chromatography (GPC). Vinyl-terminated precursor chains and tetrakis(dimethylsiloxy)silane cross-linker were vigorously stirred with a spatula and left on a rotator overnight to ensure homogeneous distribution of the components. The mixture was cured by addition of cis-dichlorobis (diethylsulfide)platinum(II) catalyst and by heating at 35 °C for three days in an oven.

It is difficult to perform a systematic series of experiments on trimodal networks due to the large number of design variables that include three molar masses and two independent molar fractions. Therefore, we have chosen to synthesize trimodal networks with varying amounts of short–medium–long precursor chains of 800–8500–91,000 g/mol. These precursor molar masses are similar to those predicted to have enhanced toughness by Erman and Mark [9]. We also examine 800–91,000 g/mol bimodal networks and unimodal networks with similar elastic moduli for comparison.

An optimal amount of tetrakis(dimethylsiloxy)silane cross-linker was used in each sample to produce networks with as few defects as possible. This is achieved in end-linked unimodal PDMS networks at a ratio of cross-linking arms to polymer chain ends r of 1.7 for M_n greater than about 10,000 g/mol [16]. Since optimal r is smaller for networks of shorter precursor molar masses [17], the ideal ratio is not obvious for bimodal or trimodal networks containing chains of widely varying precursor molar mass. Therefore, we varied r for selected 800–91,000 g/mol bimodal and 800–8500–91,000 g/mol trimodal networks and found $r = 1.7$ produced model networks with the lowest possible soluble fraction (w_{sol}) and mass swell in toluene (Q). Optimal 800–26,000 g/mol bimodal networks for cut growth testing were produced at $r = 1.1$.

2.2. Uniaxial extension tests

Samples of uniform width and thickness for simple extension tests were punched out of the cured PDMS networks. These test pieces were 0.5–1 mm thick and 4.3 mm wide. We measured elongation ratio α and engineering stress σ (force/initial cross-sectional area) at room temperature on an Instron 1125 with the clamps initially separated by 40–45 mm. Each sample was deformed at 20 mm/min, which we verified to be a slow enough crosshead speed such that the data for our model networks were independent of strain rate. Young's modulus E was calculated from the slope of the best fit line through the stress-elongation ratio data from $\alpha = 1.0$ to 1.05. Average molar mass between effective cross-links M_c was determined from:

$$M_c = 3\rho RT/E \tag{1}$$

Here, ρ is the density of the polymer, R is the gas constant, and T is absolute temperature. Young's modulus, ultimate stress σ_{max}, elongation ratio at fracture α_c, and toughness (area under σ–α curve to α_c) were recorded on 4–6 samples for each network formulation tested.

2.3. Cut growth tests

Fracture energy G_c was determined using samples with geometry for pure shear extension [18,19], where the width of the test piece must be at least 4 times the thickness and initial length [20]. Thus, we stamped out samples that were 25 mm wide and 0.5–1 mm thick, and the initial distance between the clamps l_0 was 3–4 mm. The Instron 1125 was outfitted with a wider set of clamps that could hold such a sample. For the cut growth experiments, a 6 mm edge cut was made along the width of the test pieces (perpendicular to the loading direction).

The fracture energy G_c was determined following procedures adapted from those originally developed by Rivlin and Thomas [20]. First, the stress-elongation ratio data were recorded on uncut samples of each type of network in pure shear. Each pre-cut sample was then extended at a constant crosshead speed until the crack had propagated through its entire width. The elongation ratio at which the crack began to grow in these samples α_{cg} was determined from the maximum of the force-displacement curve measured by the Instron, since the force immediately began to drop when the crack began to grow. We verified the accuracy of this method to determine α_{cg} by taking video footage of the crack propagation for selected samples. The elastically stored energy per unit volume required to initiate fracture (W_0) was calculated by integrating under the *uncut* stress–elongation ratio curve up to the α_{cg} of the corresponding *pre-cut* samples. Finally, G_c was calculated from [20]:

$$G_c = W_0 l_0 \tag{2}$$

We have attempted to measure only the threshold fracture energy of our materials through careful experimental methods. Additional contributions to G_c can come from viscous dissipation, strain-induced crystallization, and deviation of the tear path in reinforced materials [21,22]. Crystallization and deviation of the tear path are not factors in our unfilled PDMS networks. Viscous dissipation is already minimized in our model networks, since they contain relatively few dangling ends and defects [16] and room temperature is far above the glass transition temperature for PDMS ($T_g = -127$ °C). We have eliminated any remaining viscous contribution to our measured G_c by performing experiments at a low crosshead speed of 0.5 mm/min, after verifying that the stress-elongation data were identical to those taken on the same sample tested at 0.05 mm/min. At these low crosshead speeds, the propagating crack speed was slow and relatively constant instead of accelerating (as can occur when elastomers are rapidly loaded [23,24]).

The Mooney–Rivlin constants C_1 and C_2 were determined using simple extension tests on small pieces cut from the pure shear samples. Each of these samples was extended to $\alpha = 1.5$. These data were fit to the Mooney–Rivlin equation [25,26]:

$$\sigma/(\alpha - 1/\alpha^2) = 2(C_1 + C_2/\alpha) \tag{3}$$

3. Results and discussion

3.1. Toughness from uniaxial extension tests

Mechanical properties for all of the networks tested are displayed in Table 1. While the shape of the stress–strain curve was reproducible from sample to sample, each test piece broke at a slightly different α. Therefore, we report the average and standard deviation for 4–6 test pieces on each composition studied in Table 1. For clarity, we have chosen to display full stress–strain curves (Figs. 1a, 2a and 3a) for only the sample from each composition that reached the highest α before fracturing. Each series of networks has been assigned a name based on the number of molar mass distributions included and the mol% of short chains in the network. For instance, the 800–8500–91,000 g/mol trimodal network with 45–45–10 mol% of each respective chain length is referred to as T-45. Unimodal networks are distinguished by the molar mass of their precursor chains (i.e. U-4500), while a previously reported [15] 4500–91,000 g/mol bimodal series is referred to in the style B-4500-short chain mol%.

Stress–elongation ratio curves for a series of trimodal networks with increasing amounts of 91,000 g/mol chains are displayed in Fig. 1a. The 8500 g/mol chains were held constant at 20 mol% in this series to assess the effect of adding long chains at the expense of 800 g/mol chains. Not surprisingly, the elastic modulus decreases a great deal as long chains are added. As shown by the results reported in Table 1, B-80 (a bimodal network containing only 800 and 8500 g/mol chains) has mechanical properties that are almost identical to the brittle 800 g/mol unimodal network. Addition of 91,000 g/mol chains to the system greatly increases the ductility of the trimodal networks, such that T-70 can be stretched to nearly three times further than T-79. The networks with higher long chain content also show an upturn in stress at high α. Fig. 1a and Table 1 reveal that each of these trimodal elastomers break at σ_{max} values that are essentially identical. Sample T-70 absorbs the most energy before rupture because it breaks at similar σ_{max} as the other trimodal networks but can be extended to higher α_c. Average toughness vs. M_c data are displayed in Fig. 1b for this trimodal series and unimodal networks of varying precursor M_n. The lower M_c

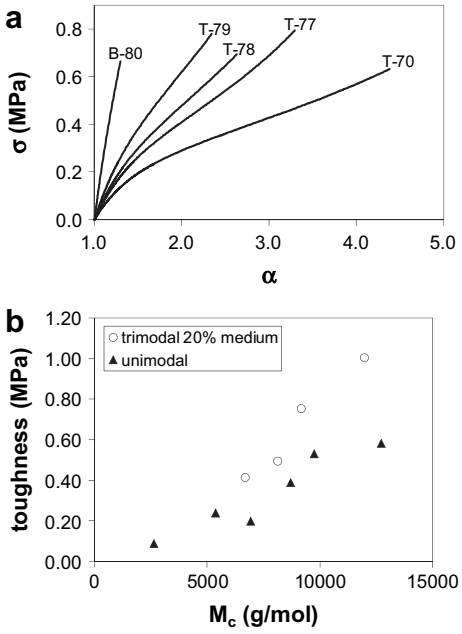

Fig. 1. a) Stress–elongation ratio curves and b) average toughness vs. M_c plots for trimodal networks with 20 mol% medium (8500 g/mol) chains. The networks are more extensible and show a stress upturn at high strain as the long chain content is increased. The toughness value of B-80 is coincident with U-800 at $M_c \sim 2700$ g/mol.

Table 1
Network Properties – Uniaxial Extension.

g/mol precursor chains	Nickname	E (MPa)	Q	w_{sol} (mass %)	Toughness (MPa)	σ_{max} (MPa)	α_c	M_c (g/mol)
Unimodal networks								
800[a]	U-800	2.72 ± 0.11	2.06	0.90	0.09 ± 0.02	0.59 ± 0.10	1.21 ± 0.09	2700
4500[a]	U-4500	1.34 ± 0.06	3.06	0.93	0.24 ± 0.01	0.57 ± 0.02	1.71 ± 0.02	5400
10,000[a]	U-10000	1.04 ± 0.03	3.16	0.34	0.20 ± 0.06	0.44 ± 0.06	1.74 ± 0.13	6900
16,500	U-16500	0.83 ± 0.02	3.94	1.01	0.39 ± 0.06	0.48 ± 0.01	2.27 ± 0.18	8700
29,000[a]	U-29000	0.74 ± 0.04	3.75	0.78	0.53 ± 0.12	0.48 ± 0.04	2.71 ± 0.24	9700
45,000	U-45000	0.57 ± 0.05	4.87	0.81	0.58 ± 0.31	0.34 ± 0.05	3.41 ± 0.93	12,700
mol% short chains (mass %)	Nickname	E (MPa)	Q	w_{sol} (mass %)	Toughness (MPa)	σ_{max} (MPa)	α_c	M_c (g/mol)
Bimodal networks 800–91,000 g/mol								
60 (1)	B-60	0.70 ± 0.01	4.49	0.64	0.42 ± 0.20	0.40 ± 0.06	2.56 ± 0.52	10,300
95 (14)	B-95	0.72 ± 0.01	4.14	1.99	0.77 ± 0.23	0.68 ± 0.15	3.09 ± 0.32	10,000
98 (30)	B-98	1.45 ± 0.02	2.63	0.48	0.89 ± 0.12	1.69 ± 0.15	2.21 ± 0.07	5000
Bimodal networks 4500–91,000 g/mol[a]								
60 (7)	B-4500-60	0.64 ± 0.03	5.17	3.74	0.64 ± 0.10	0.45 ± 0.02	3.13 ± 0.23	11,300
90 (31)	B-4500-90	0.94 ± 0.01	3.62	0.26	0.90 ± 0.09	0.79 ± 0.04	2.93 ± 0.12	7700
95 (48)	B-4500-95	1.09 ± 0.03	3.40	0.22	0.79 ± 0.09	0.82 ± 0.04	2.64 ± 0.11	6600
98 (71)	B-4500-98	1.24 ± 0.04	3.06	1.00	0.28 ± 0.09	0.57 ± 0.07	1.80 ± 0.16	5800
mol% short, medium chains (mass %)	Nickname	E (MPa)	Q	w_{sol} (mass %)	Toughness (MPa)	σ_{max} (MPa)	α_c	M_c (g/mol)
Trimodal networks 800–8500–91,000 g/mol								
80,20 (27,73)	B-80	2.75 ± 0.02	2.26	0.12	0.09 ± 0.03	0.60 ± 0.09	1.27 ± 0.05	2600
79,20 (19,53)	T-79	1.08 ± 0.02	3.35	0.81	0.41 ± 0.13	0.65 ± 0.10	2.09 ± 0.18	6700
78,20 (15,41)	T-78	0.89 ± 0.01	3.64	1.82	0.49 ± 0.16	0.61 ± 0.10	2.37 ± 0.28	8100
77,20 (12,34)	T-77	0.79 ± 0.01	3.81	0.98	0.75 ± 0.28	0.63 ± 0.14	2.92 ± 0.44	9200
70,20 (5,15)	T-70	0.60 ± 0.01	4.70	1.69	1.00 ± 0.29	0.56 ± 0.08	3.89 ± 0.53	12,000
80,10 (6,8)	T-80	0.60 ± 0.03	4.67	1.11	0.82 ± 0.43	0.52 ± 0.14	3.48 ± 0.76	12,100
65,25 (4,18)	T-65	0.77 ± 0.05	4.12	0.93	1.34 ± 0.56	0.79 ± 0.19	3.88 ± 0.84	9400
45,45 (3,29)	T-45	0.95 ± 0.02	3.70	0.18	1.62 ± 0.47	1.11 ± 0.25	3.74 ± 0.37	7600

[a] Previously reported in reference [15].

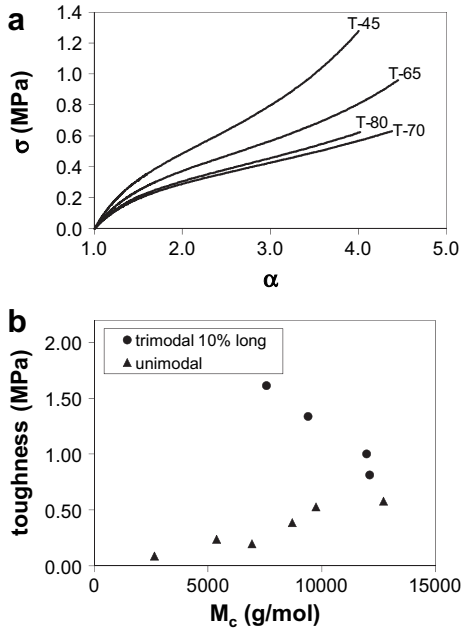

Fig. 2. a) Stress–elongation ratio curves and b) average toughness vs. M_c plots for trimodal networks with 10 mol% long (91,000 g/mol) chains. Networks T-45 and T-65 in particularly show outstanding mechanical properties when compared to unimodal networks of similar moduli.

trimodal networks only show a moderate increase in toughness over unimodal networks with similar low-strain elastic modulus (or similar M_c, equation (1)). However, the toughness values for each series begin to diverge in the more ductile networks. Therefore, networks with higher long chain content appear to be more likely to display improved ultimate properties, showing qualitative agreement with the predictions of reference [9].

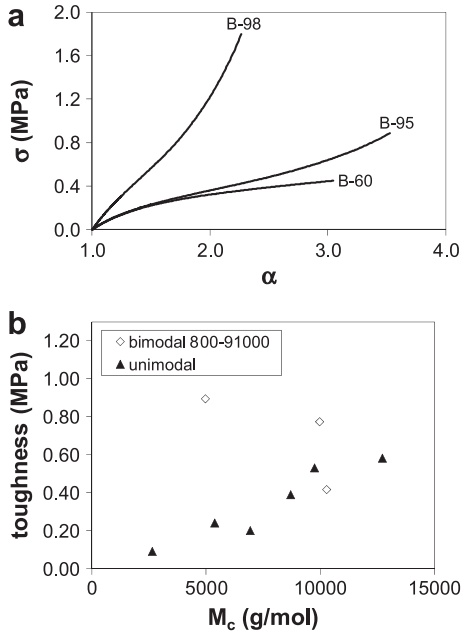

Fig. 3. a) Stress–elongation ratio curves and b) average toughness vs. M_c plots for bimodal networks with very widely separated precursor chains (800–91,000 g/mol). B-98 shows a very large stress upturn and sustains a high stress before fracture.

Based on the properties of T-70, we synthesized a series of trimodal networks with a constant 10 mol% of 91,000 g/mol chains and varying short and medium chain contributions. These networks can be classified as high long chain content systems because 10 mol% long chains correspond to 68–86 mass % in the compositions tested (Table 1). Representative stress–strain curves are shown in Fig. 2a. The networks display a relatively high elastic modulus while still maintaining extraordinary ductility. T-45 ($M_c = 7600$) in particular exhibits a noticeable upturn in stress that persists for quite some time before fracture. Therefore, it is not surprising that the toughness values for this trimodal system are far superior to the end-linked unimodal networks (Fig. 2b). In contrast to Fig. 1b, the higher toughness values for the 10 mol% 91,000 g/mol systems are found for networks with lower M_c.

In order to establish that these trimodal networks show enhanced mechanical properties, they must also be compared to analogous bimodal networks. We have already reported on the properties of a bimodal 4500–91,000 g/mol system in a previous publication [15]. These networks contain short chains that have essentially the average molar mass of the short and medium chains employed in the trimodal networks. While this bimodal system showed improvement over unimodal networks, Table 1 reveals trimodal networks with 10 mol% long chains to have superior toughness.

It is instructive to calculate overlap concentrations using the R_g of an ideal linear chain in these bimodal and trimodal networks. For instance, the overlap volume fraction concentration of 4500 g/mol chains is 0.47, which is almost identical to the mass % of short chains in B-4500-95 [15]. In the 4500–91,000 g/mol bimodal series, B-4500-90 and B-4500-95 have the highest toughness values. The overlap concentration for the medium (8500 g/mol) chains in the trimodal networks studied here is 0.35. The trimodal network with the best mechanical properties, T-45, incorporates medium chains at a mass fraction of 0.29. This is the highest concentration of 8500 g/mol chains used and the closest to their overlap concentration. Thus, the medium chains in T-45 may act similarly to the short chains in B-4500-90 – they form a connected skeleton that spans the network structure [15]. However, the trimodal networks are more ductile since these medium chains have twice the backbone length of the short chains in 4500–91,000 g/mol bimodal networks. The trimodals also contain a small amount of 800 g/mol chains, so the sweeping upturn in stress in T-45 can be interpreted as a result of the short and medium molar mass chains becoming highly stressed at high elongation ratios.

We also tested bimodal networks with very widely separated molar mass distributions (800–91,000 g/mol). The stress–elongation ratio curves and toughness vs. M_c results are shown in Fig. 3. While sample B-98 is not as ductile as B-60 or B-95, it exhibits an exceptional stress upturn and thus reaches a higher σ_{max} than any other sample examined in this study (Table 1). As seen in Fig. 3b, B-98 absorbs a large amount of energy before fracture for an end-linked PDMS network with a relatively high modulus.

To further analyze these interesting properties, stress data for B-98, T-45, and U-29000 are each normalized by their respective modulus E and plotted on a log–log plot vs. α in Fig. 4. This allows for comparison to the model of ideal rubber elasticity, which can be written as:

$$\sigma/E = (\alpha - \alpha^{-2})/3 \tag{4}$$

While each curve follows the ideal model at low strains, T-45 and U-29000 drop below this prediction at moderate elongation ratios. This typical behavior is attributed to "slippage" in inter-chain interactions (entanglements) as the network is deformed (modeled by the C_2 term in the Mooney–Rivlin equation). At high strains,

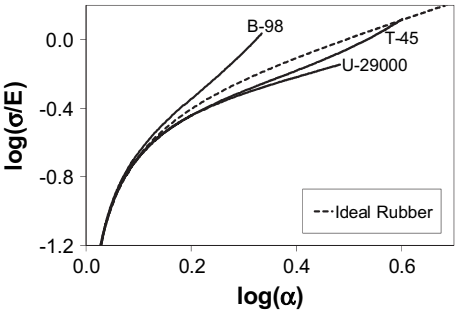

Fig. 4. Results from unimodal and multimodal networks compared to the prediction of ideal rubber elasticity. Bimodal network B-98 has a Mooney–Rivlin C_2 parameter equal to zero because it never dips below the ideal rubber prediction.

limited extensibility of the shorter chains in T-45 leads to an upturn in stress and the curve again reaches the ideal rubber prediction before fracture. The data from sample B-98 present an interesting case since they never fall below the theoretical prediction (i.e. devoid of a C_2 term). This might suggest that this network has very few chain entanglements; however, this seems impossible since 70 mass % of the chains in the system are of the "very long" 91,000 g/mol variety (Table 1). Therefore, it appears that the 800 g/mol chains approach the limit of their extensibility at low α because the load is shared between long and short chains. The increase in stress resulting from deformation of the short chains is strong enough to offset the C_2 damping of the stress–strain curve due to the long chain entanglements. Examination of Table 1 makes obvious the importance of the presence of the long chains on the mechanical properties of B-98. Sample U-800 has a high modulus but is very brittle ($\alpha_c = 1.21 \pm 0.09$), while B-98 can be stretched to about six times further on average ($\alpha_c = 2.21 \pm 0.07$).

3.2. Fracture energy from cut growth tests

Unimodal networks sweeping a wide range of precursor M_n were synthesized and tested, along with 800–26,000 g/mol bimodal networks similar to those previously shown to have enhanced mechanical properties [15] and 800–8500–97,000 g/mol trimodal networks. These trimodal networks are very similar to those described in Section 3.1, except that the long chain M_n is slightly higher. The properties of these networks are listed in Table 2 and an analogous naming convention is adopted, except for the additional prefix CG to denote cut growth samples.

3.2.1. Analysis of fracture energy of unimodal end-linked networks with the Lake-Thomas theory

The classic Lake-Thomas theory [14] directly correlates the threshold fracture energy of an elastomer with the length of the elastic strands making up the polymer network and the dissociation energy of the main-chain chemical bonds comprising these strands. This simple theory has predicted threshold strength to reasonable accuracy for a number of different elastomers [27,28]. According to Lake and Thomas [14], the fracture energy expressed as the energy to tear through a unit area can be calculated from:

$$G_c = KM^{1/2} \tag{5}$$

In this equation, M is the molar mass of the elastic strand that is to be ruptured and K is a prefactor calculated from the polymer chain properties

$$K = (3/8)^{1/2}\rho AUq^{1/2}l/M_0^{3/2} \tag{6}$$

Here, ρ is the density of the polymer, A is Avogadro's number, U is the dissociation energy of a bond along the polymer chain, q is the chain stiffness, l is the bond length, and M_0 is the molar mass of the repeat unit. Equations (5) and (6) were developed by considering ideal elastic chains with Gaussian distributions of end-to-end lengths. The derivation of this theory is available in a number of publications [14,21,28,29]. It is worth noting that nearly identical equations can be derived from a scaling argument assuming the size of the tip diameter to be on the order of the distance between adjacent cross-links [14]. The only difference found from this treatment is that the $(3/8)^{1/2}$ prefactor in equation (6) is replaced by $(8/3\pi)^{1/2}$, leading to approximately a 50% increase in the prediction for the fracture energy.

Since the Lake-Thomas treatment ignores inter-chain entanglements, the appropriate molar mass M to use in equation (5) is unclear. Is it the molar mass between actual covalent cross-links or is it M_c that takes into account the effect of entanglements on the modulus? After discussing the issue, Gent and Tobias [28] find good agreement between their threshold fracture energy data on *randomly* cross-linked PDMS networks with equations (5) and (6) using $M = M_c$. Far fewer results on end-linked PDMS are available in the literature, but tests by Yanyo and Kelley on a single end-

Table 2
Network Properties – Cut Growth.

g/mol precursor chains	Nickname	G_c (J/m^2)	α_{cg}	Q	w_{sol} (mass %)	M_c (g/mol)
Unimodal Networks						
4500	U-CG-4500	34 ± 8	1.13 ± 0.02	2.52	0.32	4000
8000	U-CG-8000	34 ± 7	1.14 ± 0.01	2.96	0.30	5400
16,500	U-CG-16500	65 ± 13	1.24 ± 0.02	3.64	0.71	7900
26,000	U-CG-26000	65 ± 8	1.26 ± 0.02	3.92	1.68	9200
29,000	U-CG-29000	82 ± 21	1.45 ± 0.08	4.57	0.82	12,000
45,000	U-CG-45000	105 ± 25	1.40 ± 0.06	4.87	0.81	12,700
mol% short chains (mass %)	Nickname	G_c (J/m^2)	α_{cg}	Q	w_{sol} (mass %)	M_c (g/mol)
Bimodal Networks 800–26,000 g/mol						
60 (4)	B-CG-60	67 ± 18	1.28 ± 0.04	3.94	0.86	8800
85 (15)	B-CG-85	65 ± 9	1.23 ± 0.02	3.40	2.23	7300
90 (22)	B-CG-90	65 ± 9	1.23 ± 0.01	3.49	2.28	7000
mol% short, medium chains (mass %)	Nickname	G_c (J/m^2)	α_{cg}	Q	w_{sol} (mass %)	M_c (g/mol)
Trimodal Networks 800–8500–97,000 g/mol						
45,45 (3,28)	T-CG-45	125 ± 19	1.36 ± 0.03	3.74	0.23	8400
65,25 (4,17)	T-CG-65	127 ± 12	1.42 ± 0.03	4.74	0.58	11,100
80,10 (6,8)	T-CG-80	122 ± 5	1.49 ± 0.03	5.36	2.63	13,600

linked unimodal network also appeared to match the theory with $M = M_c$ relatively well [30]. Calculation of M_c via equation (1) considers the low-strain modulus, where both chemical crosslink constraints and inter-chain entanglements (modeled by the C_1 and C_2 terms in the Mooney–Rivlin equation, respectively) are significant. However, chains that tear at the crack tip are expected to be in a state of high stress/strain and as shown for the unimodal network in Fig. 4, the effect of entanglements dissipates at high strain.

In Fig. 5a, fracture energy data for our end-linked unimodal networks and for the randomly cross-linked networks of Gent and Tobias are plotted versus M_c. Also plotted is the Lake-Thomas prediction for PDMS given by Eqs. (5) and (6) with $\rho = 0.97$ g/cm^3, $U = 6.1 \times 10^{-19}$ J, $q = 6.25$, $l = 0.143$ nm, $M_0 = 37$ g/mol, and $A =$ Avogadro's number. The previously reported data on randomly cross-linked networks are much better represented by the model. The data from the previously reported unimodal end-linked network with low M_c compares well with our data for similar low M_c networks. However, our experimental fracture energies become significantly higher than the theoretical prediction as M_c increases. One concern that may arise is that our results are influenced by viscoelastic relaxation [31]. However, our data were collected at a low strain rate where the measured stress is not influenced by strain rate. To verify this, we made equilibrium stress measurements at different fixed strains that reproduced the same stress levels under our selected low strain rate. We also note that for our properly end-linked elastomers (with few pendant chains), the stress levels off rapidly to higher than 98% of its initial value [32]. We expect therefore that any errors in our measured W_0 (in Eq. (2)) are negligible.

In an attempt to provide an explanation for our results, we consider analyzing our data with the original Lake-Thomas model taking M to represent the molar mass between actual covalent cross-links. To this end, we calculate M by using only the Mooney–Rivlin $2C_1$ contribution to the modulus as it represents the effect of chemical cross-links [25,26,28]:

$$M = M_c(C_1) = \rho RT/2C_1 \tag{7}$$

Fig. 5b displays G_c vs. $M_c(C_1)$ results compared with the same theoretical prediction. The unimodal end-linked network data has now shifted closer to the dashed line generated by equations (5) and (6). Also plotted as a solid line is the Lake-Thomas prediction with a prefactor of $(8/3\pi)^{1/2}$ (the alternative prefactor based on crack tip diameter).

The closer correspondence of the $M_c(C_1)$ data to the theory for the end-linked elastomers suggests that the chemical constraints are the most important factor in the fracture process of such networks. In this point of view, "slippage" of trapped entanglements at high strains causes the elastic strand length to be governed primarily by the chemical cross-links. In fact, the data for G_c vs. $M_c(C_1)$ are well predicted by the Lake-Thomas theory with a $(8/3\pi)^{1/2}$ prefactor (solid line). In cut growth tests, the stress is concentrated at the crack tip and the material in its immediate vicinity is in a highly stretched and complicated state [33]. Thus, the stretched chains that are ruptured once threshold fracture begins (those just ahead of the crack tip) have a local α that is likely much greater than α_{cg}. Here, one would expect a significant decrease in the contribution to fracture energy from inter-chain entanglements.

We now return to the results of Fig. 5a. Additional threshold fracture energy experiments on randomly cross-linked PDMS by Mazich et al. [29,34] have also correlated the characteristic elastic strand length for fracture with the entanglement spacing for PDMS. The G_c results of Gent and Tobias can also be plotted against $M_c(C_1)$ to isolate the effect of the chemical cross-links on fracture energy because these authors have provided values of the Mooney–Rivlin coefficients of their samples. However, we must now consider the influence of pendant chains on the effective density of elastic chains in each network. The Lake-Thomas theory assumes all chains to be elastic, which is a reasonable approximation for our model end-linked networks with negligible amount of defects, but not for randomly cross-linked networks. The fraction of elastic chains in randomly cross-linked networks can be estimated from the initial molar mass in the melt state $M_{n,init}$ and the molar mass between chemical cross-links $M_c(C_1)$ upon network formation (equation (7)). The ratio of $M_{n,init}$ to $M_c(C_1)$ is the average number of sections between cross-links into which each initial chain will be partitioned into. Because each initial chain will have two inelastic sections, the fraction of elastic chains f_{el} in randomly cross-linked networks can be estimated from:

$$f_{el} = \frac{M_{n,init}/M_c(C_1) - 2}{M_{n,init}/M_c(C_1)} = 1 - \frac{2}{M_{n,init}/M_c(C_1)} \tag{8}$$

The subtracted term in the equation accounts for the two ends of the initial molecule that become pendant strands upon cross-linking. The measured fracture energy $G_{c,meas}$ for the randomly cross-linked networks can be compared to the Lake-Thomas theory by adjusting the raw data to account for the fewer number of elastic chains actually crossing the fracture plane. Since the fracture plane is two-dimensional but f_{el} is a volume term, the adjustment factor must be raised to the 2/3 power:

$$G_c = (1/f_{el})^{2/3} G_{c,meas} \tag{9}$$

We note that this correction is not required for G_c vs. M_c plots (as shown in Fig. 5a) since M_c represents the molar mass of *effective* elastic strands when calculated from the elastic modulus E.

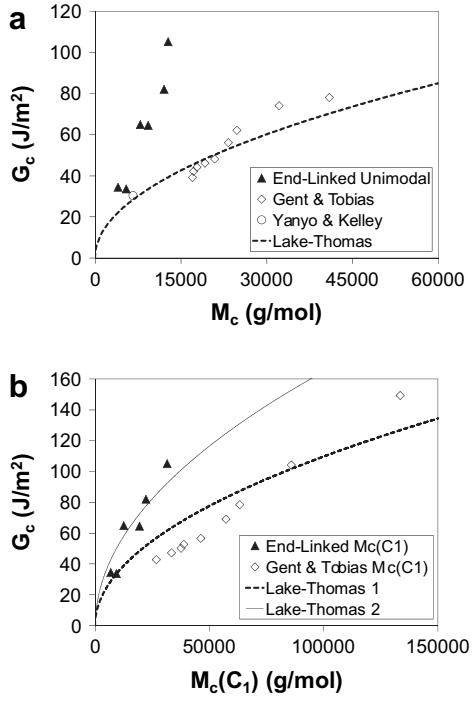

Fig. 5. Threshold fracture energy of end-linked model networks, along with results from an end-linked network (Yanyo & Kelley [30]) and randomly cross-linked networks (Gent & Tobias [28]). a) $M = M_c$ in equation (5) and b) $M = M_c(C_1)$ in equation (5). The first Lake-Thomas prediction (dashed line) uses the prefactor $(3/8)^{1/2}$, while the second (solid line) uses $(8/3\pi)^{1/2}$.

The G_c values determined from equation (9) are plotted for the Gent & Tobias data against $M_c(C_1)$ in Fig. 5b. The Lake-Thomas model with the $(3/8)^{1/2}$ prefactor still does provide an acceptable representation of these data. However, the fracture energy of end-linked networks only appears to follow the original Lake-Thomas scaling prediction with the molar mass between chemical cross-links. We suspect that the different behaviors exhibited in Fig. 5 between the randomly cross-linked networks and the end-linked networks may be due to the different structure of these networks. We examine therefore the extent of chemical cross-links relative to trapped entanglements in each type of network. As shown in the inset of Fig. 6, C_2 is considerably larger than C_1 for the majority of the randomly cross-linked networks and thus the elastic response and stored energy at low strain is dominated by trapped entanglements. On the other hand, the end-linked networks are much more highly cross-linked and C_2 is less than C_1 for most of these samples (Fig. 6). Energy storage in these networks is dominated by chemical crosslink deformation. This may explain why G_c of these networks is well correlated with the theory when the factor M is taken to be $M_c(C_1)$.

3.2.2. Comparison of unimodal and multimodal results

Values of the fracture energy G_c are plotted against M_c for unimodal, bimodal, and trimodal networks in Fig. 7. It is immediately apparent than any enhancement in G_c for multimodal networks is substantially weaker than that seen in toughness measured by uniaxial extension (Section 3.1, Figs. 2 and 3). In fact, the bimodal networks show almost identical fracture energy to unimodal networks of similar M_c, while we have shown that similar networks to B-CG-85 and B-CG-90 have enhanced toughness in simple extension [15]. These results are somewhat at odds with some previously reported studies. For instance, Yanyo and Kelley found increased fracture energy in a bimodal network as compared to unimodal, but this was only for a single sample of each and the networks were of relatively poor quality ($w_{sol} \sim 5\%$) [30]. Other researchers have found the fracture energy of bimodal networks to peak at certain short chain compositions [35,36], but these experiments did not compare to equivalent unimodal networks and the network qualities were not reported. The trimodal networks studied here fared slightly better than the unimodal networks, but only T-CG-45 (and perhaps T-CG-65) has a G_c value that is distinctly higher than the corresponding unimodal networks.

Elongation ratios at fracture α_c for the uniaxial extension tests (Section 3.1) are plotted against M_c in Fig. 8a, while average elongation ratios at the moment when crack growth began in cut growth testing α_{cg} are displayed in Fig. 8b. In simple extension, the bimodal and trimodal networks usually reach higher α_c before fracture than unimodal networks with similar values of elastic modulus. These results reiterate that enhanced mechanical properties in multimodal networks are manifested at high strains [15]. When a pre-cut sample is prepared, network fracture begins at a much lower elongation ratio since the stress is concentrated at the crack tip. While it is difficult to speculate on the sharpness or bluntness of natural imperfections, enclosed flaws are considered less serious stress raisers than edge cuts [37]. Since the pre-cut samples in the tests reported here always utilize edge cuts and we expect the crack tip to be sharp, it is not surprising that the α_{cg} values from Fig. 8b are much lower than the α_c values from Fig. 8a. In the cut growth tests, α_{cg} follows roughly the same trend with M_c whether the networks are unimodal or multimodal. The resulting G_c values are similar for most networks with similar M_c except for the trimodal networks that have slightly higher values. We suspect that the shape of the crack tip as the crack grows plays an important role in these results.

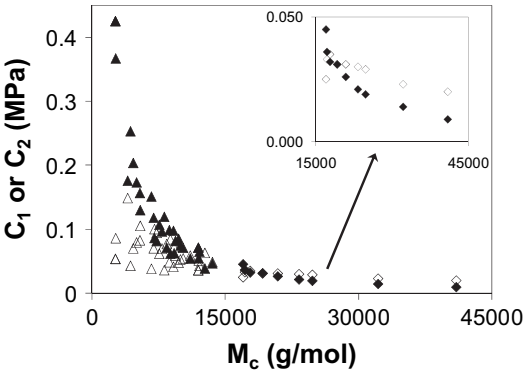

Fig. 6. Mooney–Rivlin parameters C_1 and C_2 vs. M_c for end-linked networks reported here (triangles) and randomly cross-linked networks from Gent & Tobias (diamonds) [28]. Values of C_1 are represented by filled symbols and those of C_2 by open symbols.

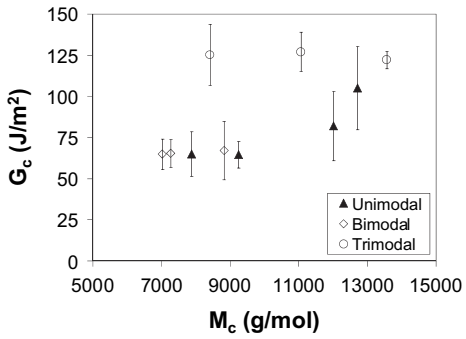

Fig. 7. Fracture energy vs. M_c for unimodal and multimodal networks. Degree of enhancement in G_c for trimodal networks is much milder than in toughness measured by uniaxial extension.

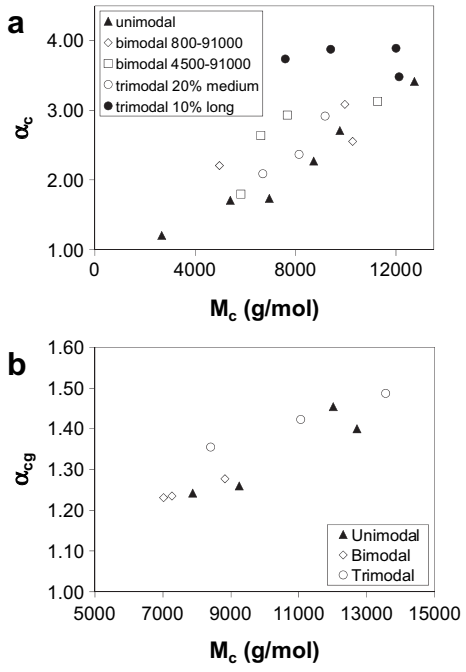

Fig. 8. Average elongation ratio at fracture for a) uniaxial extension and b) cut growth experiments. Multimodal networks can usually be stretched farther than unimodal networks with similar M_c in uniaxial extension. Note the different scales on each ordinate.

4. Conclusion

Unimodal, bimodal, and trimodal networks are investigated using uniaxial extension and pure shear cut growth experiments. Trimodal networks can show outstanding mechanical properties in simple extension when the majority of the volume fraction of the networks is taken up by long chains. Such elastomers can be extended to a large elongation ratio in uniaxial extension before fracture and have a large upturn in stress at high elongation, resulting in toughness values that are much higher than unimodal networks with similar elastic modulus. Bimodal networks with very widely separated chain lengths are not quite as tough as trimodal networks, but can sustain high stress before fracture when the short chains reach 98 mol% in the system. The enhanced mechanical properties in multimodal networks are attributed to the ability of the shorter chains to sustain most of the applied stress, while the more flexible long chains provide ductility. These properties are maximized when the short or medium chains are near their overlap concentration, such that the resulting microstructure consists of an interconnected skeleton of the shorter chains with intermittent regions heavily populated by the long chains.

Multimodal networks do not show the same degree of improvement in threshold fracture energy. This is a consequence of the inability of the bimodal or trimodal elastomers to reach higher elongation ratios at crack growth onset than unimodal networks with similar low-strain properties. Unimodal network fracture energies correlate closely to predictions from the Lake-Thomas theory [14] when the pertinent elastic chain length is taken to be the distance between chemical cross-links. Therefore, entanglements appear to have less influence on the fracture process in these end-linked model networks. We conclude however that the relative roles of cross-links, entanglements and pendant chains on the fracture energy of elastomers are not yet fully understood.

Acknowledgements

We thank Chung-Yuen Hui for numerous helpful tips and discussions. This work was supported by the National Science Foundation Polymers Program under grant DMR-0705565. This work made use of the Cornell Center for Materials Research Shared Experimental Facilities supported through the National Science Foundation Materials Research Science and Engineering Centers program (Award DMR-0520404).

References

[1] Mark JE. J Phys Chem B 2003;107:903–13.
[2] Andrady AL, Llorente MA, Mark JE. J Chem Phys 1980;72:2282–90.
[3] Llorente MA, Andrady AL, Mark JE. J Polym Sci Pol Phys 1981;19:621–30.
[4] Mark JE, Tang M-Y. J Polym Sci Pol Phys 1984;22:1849–55.
[5] Mark JE. Acc Chem Res 1994;27:271–8.
[6] Genesky GD, Aguilera-Mercado BM, Duncan TM, Cohen C, Escobedo FA. Macromolecules, submitted for publication.
[7] Sakrak G, Bahar I, Erman B. Macromol Theory Simul 1994;3:151.
[8] Madkour T, Mark JE. J Macromol Sci Macromol Rep 1994;A31:153–60.
[9] Erman B, Mark JE. Macromolecules 1998;31:3099–103.
[10] Giuliani JR, Gjersing EL, Chinn SC, Jones TV, Wilson TS, Alviso CT, et al. J Phys Chem B 2007;111:12977–84.
[11] Gjersing E, Chinn S, Giuliani JR, Herberg J, Maxwell RS, Eastwood E, et al. Macromolecules 2007;40:4953.
[12] Saalwächter KJ. Am Chem Soc 2003;125:14684–5.
[13] Saalwächter K, Sommer J-U. Macromol Rapid Commun 2007;28:1455–65.
[14] Lake GJ, Thomas AG. P R Soc Lond A Mat 1967;300:108–19.
[15] Genesky GD, Aguilera-Mercado BM, Bhawe DM, Escobedo FA, Cohen C. Macromolecules 2008;41:8231–41.
[16] Patel SK, Malone S, Cohen C, Gillmor J, Colby R. Macromolecules 1992;25:5241–51.
[17] Takahashi H, Shibyama M, Fujisawa H, Noruma S. Macromolecules 1995;28:8824–8.
[18] Takigawa T, Yamasaki S, Urayama K, Takahashi M, Masuda T. Rheol Acta 1996;35:288–95.
[19] Urayama K, Ogasawara S, Takigawa T. Polymer 2006;47:6868–73.
[20] Rivlin RS, Thomas AG. J Polym Sci 1953;10:291–318.
[21] Bhowmick K. J Macromol Sci R M C 1998;C28:339–70.
[22] Lake GJ. Rubber Chem Technol 1995;68:435–60.
[23] Baumberger T, Caroli C, Martina D. Eur Phys J E 2006;21:81–9.
[24] Baumberger T, Caroli C, Martina D. Nat Mater 2006;5:552–5.
[25] Mooney MJ. Appl Phys 1940;11:582–92.
[26] Rivlin RS. Philos Trans R Soc 1948;A241:379–97.
[27] Ahagon A, Gent AN. J Polym Sci Pol Phys 1975;13:1903–11.
[28] Gent AN, Tobias RH. J Polym Sci Pol Phys 1982;20:2051–8.
[29] Mazich KA, Samus MA. Macromolecules 1990;23:2478–83.
[30] Yanyo LC, Kelley FN. Rubber Chem Technol 1987;60:78–88.
[31] Plazek DJ, Gu G-F, Stacer RG, Su L-J, Von Merwall ED, Kelley FN. J Mater Sci 1988;23:1289–300.
[32] Batra A, Cohen C, Archer LA. Macromolecules 2005;38:7174–80.
[33] Hui C-Y, Jagota A, Bennison SJ, Londono JD. P R Soc Lond A Mat 2003;459:1489–516.
[34] Mazich KA, Samus MA, Smith CA, Rossi G. Macromolecules 1991;24:2766–9.
[35] Smith TL, Haidar B, Hedrick JL. Rubber Chem Technol 1990;63:256–64.
[36] Shah GB, Winter RW. Macromol Chem Physic 1996;197:2201–8.
[37] Gent AN. Strength of elastomers. In: Mark JE, Erman B, Eirich FR, editors. Science and technology of rubber. 2nd ed. San Diego: Academic Press; 1994. p. 471–512.